Iranian Journal of Science and Technology, Transactions of Mechanical Engineering (2023) 47:469–479
https://doi.org/10.1007/s40997-022-00547-4

RESEARCH PAPER

The Local Dependence of Bubble Breakup for Different Impeller Geometries in a Stirred Tank

Muayad F. Hamad[1] · Basim O. Hasan[1] · Hasan Sh. Majdi[2] · Richard A. Craig[3] · Hussein A. Alabdly[1] · Mustafa M. Hathal[4]

Received: 1 May 2021 / Accepted: 4 October 2022 / Published online: 18 October 2022

Abstract
This work presents an investigation into the effect of impeller geometry on the local bubble breakage behavior in a stirred tank. The relative breakage location and local number of produced daughter bubbles (fragments) were investigated using a high-speed imaging method. Three impeller geometries were used for a range of impeller Reynolds numbers (Re) (18380–40830). The impellor geometries used were: 4-flat blades, 4-twisted blades, and 2-flat blades. The results revealed that the number of breakages around the impeller is dependent on the impeller geometry and Re. At lower Re, most breakages occurred close to the tip of the blades in locations near the entry to the impellor region. For higher Re, the rotational motion of the fluid drives the mother and daughter bubbles into different regions around the impeller before breaking up. The highest number of daughter bubbles was observed to be generated close to the blade's tips of 4-flat blades impeller (average of 8.3). The lowest number of daughter bubbles was observed to occur for the 4-twisted blades (average 2.7). The highest percentage of local bubble breakages and the highest number of resulting daughter bubbles were observed for the 4-flat bladed impeller for all Re (reached up to 90% for highest Re).

Keywords Bubble · Breakage · Breakage location · Impeller geometry · Stirred tank

1 Introduction

Gas–liquid and liquid–liquid dispersions are of practical importance in a variety of industrial applications such as fermentation, mixing, extractions, biochemical reactors, and gas–liquid and liquid–liquid separation in the petroleum processes (Hallaile and Merchuk 2007; Azizi et al. 2019, Feng et al. 2019). The characterization of local breakage of bubbles and drops in stirred tanks has a scientific significance for improving processing operations through better tank and impeller designs.

The geometry and design of the impeller blades have an important influence on the flow patterns around the impeller which in turn affects the breakage rate and location and number of fragments (daughter bubbles) produced. Simple modifications to blade geometry can cause an appreciable effect on the bubble breakage behavior (Martin 2008). The geometry affects breakage probability, time, and location relative to the impeller. The bubble size distribution in stirred tank is very important as it determines the surface area of contact between the continuous and dispersed phase. The use of efficient impeller geometries determines to a wide extent the bubble size distribution as it affects the breakup process. The small bubble size is generally required for effective mass and heat transport in two-phase flow systems. The size distribution is also a direct function of the impeller speed and physical properties of both continuous and dispersed phase such as viscosity and density (Mesa and Brito-Parada 2020). The use of high-speed imaging and a deeper understanding of local breakage behavior in stirred tanks can be attained (Solsvik et al. 2016; Hasan 2017b).

✉ Basim O. Hasan
basimohasan13@gmail.com;
basimhasan2017@eng.nahrainuniv.edu.iq

[1] Department of Chemical Engineering, Al-Nahrain University, Baghdad, Iraq

[2] Department of Chemical Engineering and Petroleum Industries, Al-Mustaqbal University College, Hillah, Iraq

[3] School of Mechanical Engineering, The University of Adelaide, Adelaide, Australia

[4] Department of Environment, Industrial Development and Management, The Ministry of Industry and Minerals, Baghdad, Iraq

The turbulent flow structure around the impeller has been studied by several authors (e.g., Hartmann et al. 2004; Maass et al. 2011; Zamiri and Chung 2018). Those studies reported unpredictable behavior of the bubble in the impeller region due to the complicated hydrodynamics around the impeller. Ameur and Vial (2020a, b) found that the presence of a cut in the blade tip, affect strongly the flow patterns around that impeller. Ameur (2019, 2020a, b) reported that the modifications in the blade geometry improved the mixing characteristics in a stirred tank by affecting the hydrodynamics around the blade tip.

Hartmann et al. (2004) theoretically investigated the eddy viscosity and turbulent kinetic energy around the blade of a Rushton turbine. Their flat bladed impeller had a diameter $Di = 50$ mm and blade width of 0.2Di (10 mm). As can be seen in Fig. 1b, the maximum turbulent viscosity is within 0.2Di radially from the blade's tip. Beyond this distance, it drops by 50% and then a further 78% by 0.5Di. The eddy viscosity is very different above and below the blade (z-direction), with a 95% change (compared to the tip) within 0.1Di. The authors found that the turbulent kinetic energy is a maximum at the blade's tip until a distance of 0.5Di where it drops considerably.

Using an impeller to tank diameter ratio of $D/T = 0.35$, and blade width to impeller diameter of $W/D = 0.25$, Solsvik and Jakobsen (2015), found that the bubble breakage active area is the region between the blade's tip and the wall baffles. They reported that about 80% of final breakages occur within this region for a constant stirring speed.

Using a test rig with dimensions similar to that used by Solsvik and Jakobsen (2015) and Hasan (2018), reported that the bubble breakage probability is a function of the injection location of mother bubble relative to the impeller. Hasan (2018) reported that up to 70% of breakages occur between the blade's tip and a distance of 35% of impeller diameter close to the wall baffles, this percentage decreases to zero. The breakage probability and distribution of breakage locations are a function of factors such as, blade dimensions and

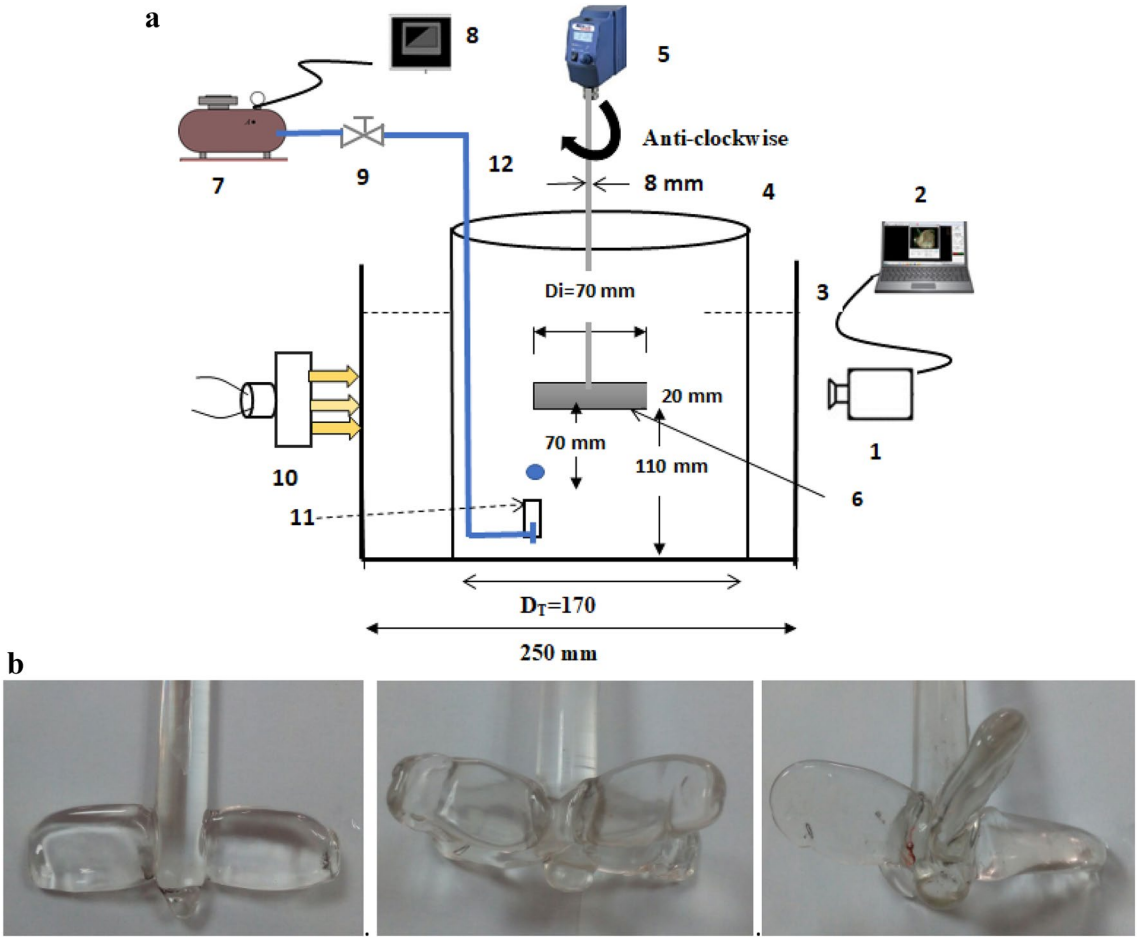

Fig. 1 **a** Experimental apparatus: 1—high-speed camera, 2—computer, 3—outer glass tank, 4—inner cylindrical tank, 5—stirrer, 6—impeller, 7—air pump, 8—air regulator, 9—gas control valve, 10—LED lamp, 11—external injection tube, and 12—injection tube. **b** Impeller geometries investigated, 1) 2-flat blade impeller, 2) 4-flat blade impeller, and 3) 4-twisted blade impeller

geometry, impeller power input, mother bubble size, injection location, and impeller to tank diameter ratio. Therefore, continued investigation and analyses are required for successful characterization of a stirred tank system.

In stirred tank, blades cavitation may occur when the impeller pushes the liquid from the tank's center toward the tank's wall (Buss et al. 2017). In the cavitation process, the local pressure of the liquid drop is lower than the vapor pressure. This causes the liquid to partial evaporates to form cavities which enlarge as the pressure keeps at low level. This size of these cavities increases with time until the damage. When the cavities are damaged, a high amount of energy is produced leading to increase the temperature and pressure. The cavity damage may produce a high-velocity liquid jet which results in a large shearing effect (Kausley et al. 2018).

Experimental determination of local breakup behavior in a stirred tank is difficult to characterize due to large variation in kinetic energy around the impeller, complicated bubble trajectory, getting consistent sized bubbles, and the number of bubbles required to make substantiated claims. These are all required for evaluation of the effect of different impeller designs on bubble breakage behavior at different impeller speeds. Another challenging problem is to obtain quality images of the bubbles at the higher impeller rotational speeds. Single bubble breakage experiments are the most useful method for obtaining detailed information about the local breakage behavior (Oliveira et al. 2003).

The use of high-speed imaging method for bubble or drops breakup studies in turbulent field has several advantages and disadvantage compared to other methods such as sampling method (Alves et al. 2020), light scattering measurements (Abbaszadeh et al. 2021), and conductivity probe method (Shi et al, 2020). The advantages are that the high-speed cameras can provide direct measurement and instantaneous local images of fluid particles under high turbulence level. The dynamic behavior and shape deformation can be easily studied and analyzed by high-speed imaging (Hasan 2017; Forgia et al. 2021). On the other hand, the limitations include: inexact volume estimation of particles using two-dimensional images, difficulty in detecting very small particles, lack of image sharpness depending on the particle position and illumination, and not suitable for high dispersed phase fraction due to overlapping of fluid particles.

Understanding the local breakup behavior assists to specify the optimum design considerations and operating conditions for obtaining high mixing efficiency in stirred tanks. Due to complex hydrodynamics of stirred tanks, studies concerning this issue are still not sufficient for comprehensive characterization of such system. The aim of this work is to identify the local breakage behavior relative to different impeller geometries, for a range of power inputs using a high-speed imaging method. In addition, it is aimed to determine the number of fragments produced from each breakage at the different locations of the different impeller geometries investigated.

2 Experimental Work

Figure 1a shows a sketch of the experimental rig. The rig comprises an un-baffled cylindrical Perspex tank which contains distilled water as a continuous phase. To prevent image distortion the cylindrical tank was placed inside a rectangular tank also containing water. The main components of the apparatus include the impeller (which is located centrally in the tank), a high-speed camera, a LED light for illumination, an air pump for bubble injection, a Teflon bubble injection tube, a control valve for the control of the bubble injection rate, and Table 1 lists the characteristic dimensions of the experimental system components.

Three different glass impellers were used (Fig. 1b); a 4-flat blades impeller, a 4-twisted blades impeller, and a 2-flat blades impeller. These are shown in Fig. 2b. The use of glass assists with image-tracking of the bubbles when their trajectory went behind or between the blades.

The Phantom Miro-C110 high-speed camera that was used, has a resolution of 1280 × 800 pixel and a frame rate of 1000 frames per second was used with exposure time of 100 µs. This frame rate was sufficient to follow up the trajectory and observe the breakage events and number of daughter bubbles produced for the range of impeller speeds investigated.

The impeller stirring speeds were 180 rpm and 400 rpm which correspond to Reynolds numbers (based on the impeller diameter) of 18,380 and 40,830, respectively. The Reynolds number (Re) is calculated using (Harriott, 2001; Slaiman et al. 2008):

$$\mathrm{Re}_i = \frac{\rho N D_i^2}{\mu} \tag{1}$$

where ρ is the continuous phase density, N is the impeller rotational speed, D_i is the impeller diameter and µ is the

Table 1 Dimensions of experimental rig components

Components	Dimensions
Cylindrical tank	Diameter = 170 mm, Height = 300 mm
Rectangular tank	Length = Width = Height = 250 mm
Impellers diameter	70 mm
Impeller shaft diam	8 mm
Blades	Length = 30 mm, Width = 20 mm, Thickness = 3 mm
Injection tube	Inside diameter = 3.8 mm, Outside diameter = 4.2 mm

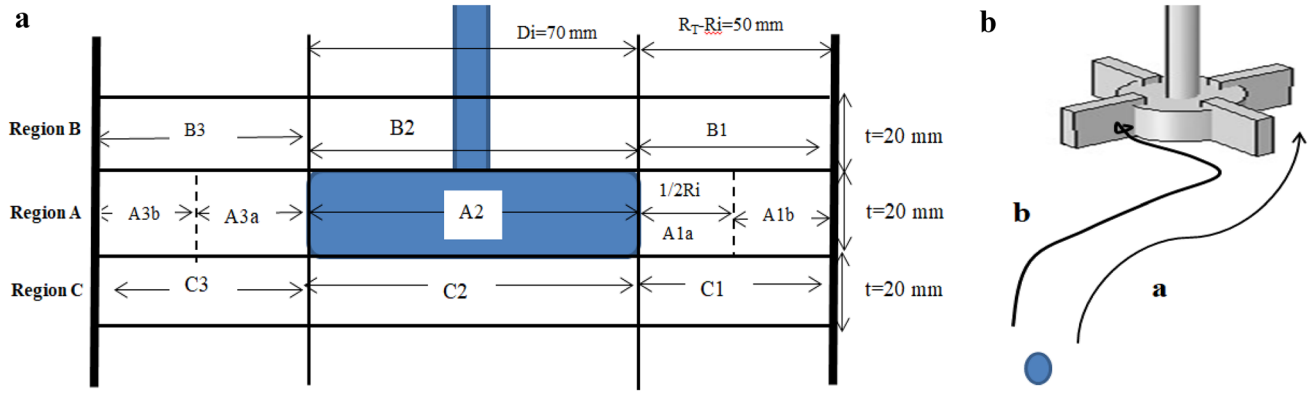

Fig. 2 **a** Division of impeller region into 11 sub-regions for identifying breakage locations. **b** Trajectories of the injected mother bubble after release from the injection tube, a) lower Re and b) higher Re

continuous phase viscosity. This range of Re was selected because these Re values express the breakup behavior at low and high Re (or stirring speed). For lower values, the breakups are very little and not worth investigating. For higher Re values the stirring becomes very high and the water in the tank becomes unstable and air bubbles from the atmospheres are sucked inside the water.

The experimental procedure was the same as described by Hasan (2017a, 2018). The mother bubble was injected at 70 mm below the blade's tip and a distance of 50 mm from the tank's wall. The injection position was selected after performing some primary tests to ensure that most injected bubbles go to the impeller region. The injection rate of mother bubble was 1 bubble per 3 s. The diameter of each released mother bubble was measured to be approximately 4.5 ± 0.1 mm. The mother bubble size was controlled by using a glass tube surrounding the exit of the injection tube to shield the bubble during release (Hasan and Krakau, 2017).

After injecting the mother bubble, its trajectory and breakage locations were recorded for each impeller geometry and impeller speed. At least 500 injection tests were considered for each of the experimental conditions. Breakage events that were not reported include recordings in which bubbles went away impeller region or when the daughter bubbles overlapped.

Breakage probability (BP%) is calculated using (Solsvik and Jakobsen 2015; Maass and Kraume 2012):

$$\mathrm{BP}\ \% \ = \frac{n}{n_T} \times 100 \tag{2}$$

n is the number of breakage events, and n_T is the number of bubble injections.

The average number of fragments (or daughter bubbles) is calculated using:

$$n_{\mathrm{a}} = \frac{n_r}{n} \tag{3}$$

where n_{a} is the average mean number of fragments and n_{r} the summation of daughter bubbles produced from n breakage events.

The uncertainty of the experimental results was calculated using the method presented in Moffat (1988). The percent deviation ($\mathrm{Y_i}$) is calculated as:

$$\mathrm{Y_i} = \mathrm{Y_{i,a}(measured)} \pm \delta \mathrm{Y_{i,m}} \tag{4}$$

where $\mathrm{Y_{i,a}}$ (measured) is the mean of N measurements and $\delta \mathrm{Y_{i,a}}$ is the mean deviation from the mean value representing the uncertainty. The percent (%) deviation is therefore calculated as:

$$\%\ \text{deviation} = \frac{\delta Y_{\mathrm{i,a}}}{\mathrm{Y_{i,a}(measured)}} \times 100. \tag{5}$$

The uncertainty of the experimental measurements as a percentage deviation is presented in Table 2.

Table 2 Uncertainty of experimental variables and results expressed as a percent deviation

Variable	Percent deviation
Stirring speed, rpm	±1.5%
Mother bubble diameter, mm	±3.2% (at maximum Re) ±1.3% (at minimum Re)
Average number of fragments	±20% (at maximum Re) ±3.4% (at minimum Re)
Room temperature, °C	±3.0%

3 Results and Discussion

3.1 Bubble Trajectories and Breakage Locations

To understand the local dynamic behavior of bubbles breakage and identify the relative breakage locations, the area around the impeller has been divided into 3 main regions and 11 sub-regions, as shown in Fig. 2a. Region A is the region extends in the level of blades from the tank's wall, Region B above the impeller, and Region C below the impeller. Region A is most breakage active region because it includes the high energy dissipation rat and the high shear regions close to the blade's tip. Therefore, it is divided into five sub-regions A1a, A1b, A2, A3a, and A3b. Regions B and C are divided into three sub-regions each; as shown in Fig. 2a.

After injecting the mother bubble below the impeller, it was observed that the bubble often approached the impeller following one of two trajectories shown in Fig. 2b. Trajectory 'a' was often observed for lower Re, in which the bubble travels in the direction of fluid flow caused by the impeller's anti-clockwise rotation direction and therefore approaches the impeller from sub-regions C1 or C2. For higher Re trajectory 'b' was often followed. The increased impeller rotational speed caused higher turbulence level and therefore the injected bubble circulated more taking a tortuous path before approaching the impeller from the left hand side through sub-regions C3 and D3. The bubble then frequently continued its trajectory through to sub-regions C2 and C3.

3.2 Flat Blades Impeller

The results from the experiments conducted using the 2-flat bladed impeller indicate that the location of the first and last bubble breakage events are strongly dependent on the Re. Figure 3 shows typical examples for first breakage locations around the impeller. Figure 4 shows typical examples of last breakage locations around the impeller.

Figure 5 a and b shows the percentage of breakages at different locations around the impeller for both low and high Re values, respectively. It can be seen from Fig. 5a that the majority of first breakages occur at locations A2 (57%) and B2 (36%). This is because at low Re these sub-regions are the entrance region of the injected mother bubble to the impeller region as shown by trajectory 'a' in Fig. 2b. When the bubble approaches the impeller it is exposed to a high-velocity gradient which causes a shearing effect on the bubble's surface. There is also higher turbulence in this region which results in the bubble breaking into number of fragments (Andersson and Andesson 2006; Liao and Locus 2009; Hasan 2017a).

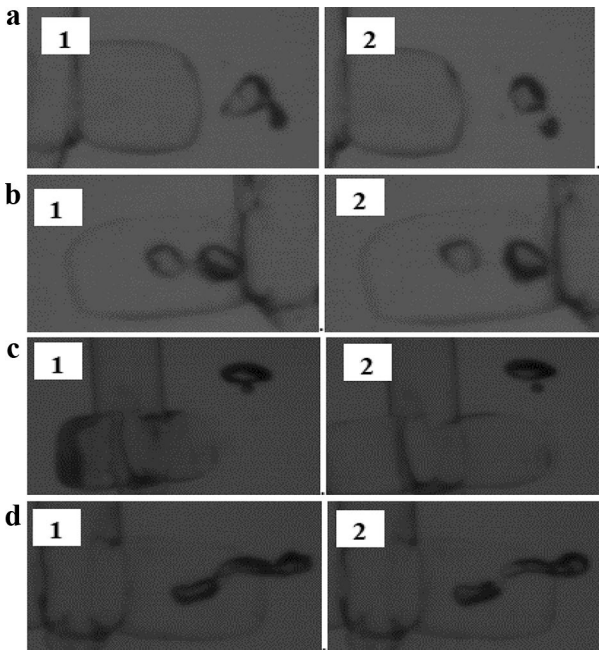

Fig. 3 First breakage locations for the 2-flat blades impeller at Re = 29,600: **a** sub-region A2, **b** sub-region C2, **c** sub-region B1, and **d** sub-region B2

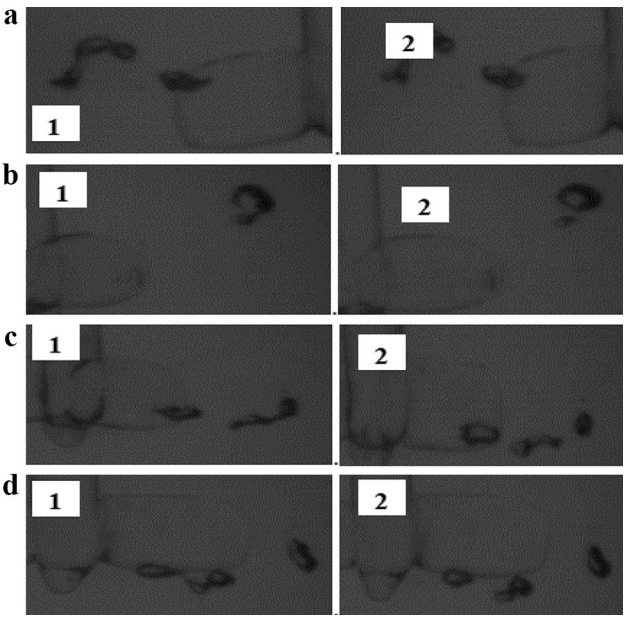

Fig. 4 Last breakage locations for the 2-flat blades impeller for Re = 40,830 at **a** sub-region D2, **b** sub-region A1, **c** sub-region A2, and **d** sub-region B2

After the first breakage, the daughter bubble(s) often stayed with the impeller band sub-regions—suffixed '2' occasionally resulting in further breakup depending on the local turbulent level. Figure 5a indicates that most of

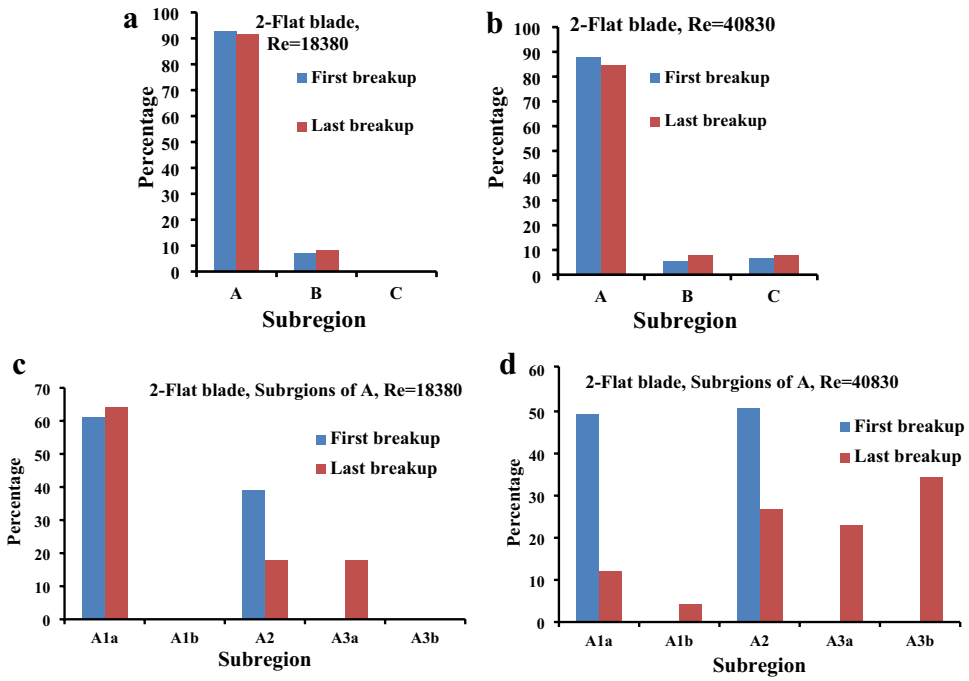

Fig. 5 Percentages of first and last breakups at different locations around the 2-flat blades impeller at **a** Re = 18,380 and **b** Re = 40,830. **c** Percentages of first and last breakages in sub-regions of A for 2-flat blades impeller at Re = 18,380. **d** Percentages of first and last breakages in sub-regions of A for 2-flat blades impeller at Re = 40,830

the last breakages occurred in sub-regions A2 (58%) and B2 (17%). This is because it was observed that at low Re, when the bubble breaks into smaller fragments (daughter bubbles), the turbulence level is not high enough to further break these smaller fragments. The kinetic energy required to break the smaller bubbles is larger than that for large size (Hasan, 2017b). Only about 17% of last breakages occur at sub-region D2, which is considered to be due to the flow currents taking the daughter bubbles away from the first breakage regions.

For the high stirring speed resulting in Re = 40,830, Fig. 5b shows that the most first breakages occur at sub-regions A2 (43%) and B2 (39%). There were very few first breakages observed in sub-regions A3 (7%), C2 (5.4%), A1 (2.7%), and B1 (2.7%). The diversity in first breakup sub-region for higher Re is considered to be because of the high strength of flow currents around the impeller which moves the mother bubbles into the different regions.

Figure 5b indicates that for higher Re, the sub-region locations of last breakages are greater than for lower Re. The majority of last breakages occurred at D2 (48%), then followed by 13% at C2 and A2, and then 9% at B2. Sub-regions A1, A3, B1, and B3 all had percentages less than 5%. The high dispersion of last breakage events is ascribed to high local intensity of turbulent eddies at higher Re which transfer the initially formed daughter bubbles into different areas before breaking them further.

Several different mechanisms have been proposed for bubble breakage in a stirred tank by previous studies (Hinze 1955; Kumar et al. 1998; Liao and Locus 2009; Martin 2008; Hasan and Krakau 2017). The leading mechanism theory which causes the most breakage is when the bubble/drop comes into contact with turbulent eddies that possess enough energy to overcome the cohesive forces that hold the bubble entity (Hinze 1955; Andersson and Andersson 2006; Liao and Locus 2009). The second mechanism theory is that the breakage occurs by the effects of the high shear layer at the surface of the impeller blade. The third mechanism suggests that the breakage occurs due to interfacial stability, which is due to the large density difference between the dispersed phase (bubble or drop) and continuous phase (Liao and Locus 2009). Breakage through collision between the bubble and the impeller blade is a fourth mechanism that has been reported by some authors (Martin 2008; Hasan et al. 2021). Therefore, in general, high breakage percentage is observed close to the blade tip due to high local energy dissipation rate at this location and also high shearing effect. In addition, the low breakage percentage observed above the impeller (Region 1) is also ascribed to the two reasons. First is lower energy dissipation rate in this region (Hartmann et al. 2004; Huchet et al. 2009). Second, the probability of mother bubble to reach this region is often little, because it either breaks up into smaller fragments which are more difficult to break up further or the mother bubble is driven by flow current horizontally.

Figure 5c presents the local breakage percent in different sub-regions of Region A for lower Re=18380. It indicates that the highest percentage of first and last breakages (about 60%) is at sub-region A1a close to the impeller tip. In sub-region A2 in between the blades, 39% of first breakage occurs and 18% of last breakages. In sub-region A3 which is away from the bubble entry region, there are no

first breakages and low percentages of last breakage. This indicates that at the blades tip close to the bubble entry region the number of breakages is highest. Away from bubble entry region, the number of breakages is low even at the blade's tip.

For higher Re=40830, Figure 5d reveals that the percentage of first breakages is still highest at the blades tip at sub-region A1a and at in between the blades at A2. However, the last breakages occur indifferent sub-regions around the impeller due to high turbulence level and high energy dissipated from the impeller. It can be seen that the highest percentage of last breakages is at sub-region A3b which is away from the impeller tip and from bubble entry to the impeller region. The highly rotating flow currents drive the mother bubble and the produced daughter bubbles into different regions around the impeller which causes an increase in the number of breakages away from blade's tip. The high level of energy dissipation rate associated with high Re assists to cause breakages away from the blades tip (Solsvik and Jakobsen 2015; Hasan 2018).

3.3 Flat Blades Impeller

The results from the experiments conducted using the 4-flat bladed impeller indicate that there is one dominant region that the first bubble breakage event occurs and then a dominant, but different, region for the last bubble breakage event. Figure 6a through c shows a series of images as typical examples of the bubble breakages around the 4-flat blades impeller. It can be seen that significant elongation of the mother bubble is occurring before breakage occurs forming two daughter bubbles for the lower Re of 29,600. It is also seen that the trajectory of the bubbles for the lower Re is in vertical direction. This is considered to be due to the buoyancy force raising the bubble through the continuous phase. This is mostly observed at lower Re, while at high Re (as in Fig. 6c), the bubble trajectory in the impeller region tends to be horizontal. The number of daughter bubbles for the higher Re is also seen in Fig. 6c to be significantly greater than for the lower Re.

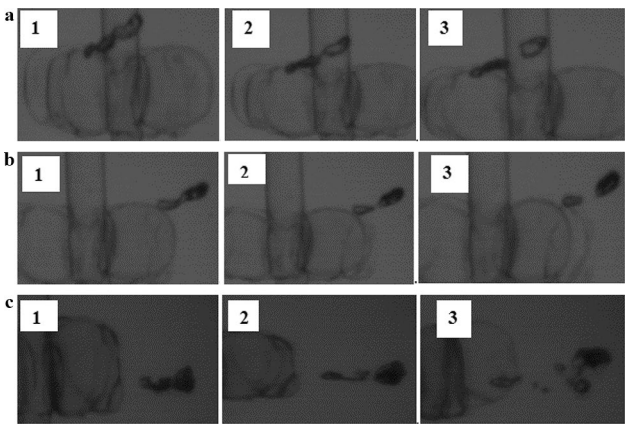

Fig. 6 **a** First breakage at sub-region C1, 4-flat blades impeller, Re = 29,600. **b** First breakage at sub-region A1, 4-flat blades impeller, Re = 29,600. **c** First and last breakage at A2, 4-flat blades impeller Re = 40,830

Figure 7a presents the first and last breakage locations for the 4-flat bladed impeller at the lower Re. It is evident that sub-region A2 has the majority of first breakages with 70.6%, followed by B1 (11.8%), B2 (8.8%) and then A1 with around 8%. Sub-region A2 has the greatest number of breakages because the flow pattern of the continuous phase around this impeller drives a majority of mother bubbles into this sub-region after release from the injection tube.

The last breakups are also occurring mainly in A2, A1, B1, and B2. So the first and last breakage sub-regions are close to each other because the power input is low and thus the produced fragments are not pushed very far from the location of first breakups and they may break up in the same locations of first breakage.

Figure 7b shows the first and last breakage locations for the higher Re. The data indicates that the first breakages are concentrated in sub-regions B2, A2, C2, and A1. The high percentage of breakage in B2 and A2 is ascribed to the fact that these regions are the main trajectory regions for the mother bubbles for the higher Re, as shown by trajectory 'b' in Fig. 2b. The large mother bubble often approaches these sub-regions and therefore the probability of breakage is also high. The first breakages occurring in A1 and B1 were observed to be the major breakage sub-regions because elongation was occurring in sub-regions A2 and B2, but breakage didn't actually occur until it had passed through to A1 and B1. Appreciable breakage percentage is also seen in the sub-regions A2 and B2 because of high shearing effect of blades at these areas.

Figure 7b also shows that the majority of last breakages occur at sub-region D2 (47.5%). This is because the flow currents at higher Re cause the successive breakages to travel a lot further and thus flow through to sub-region D2 before the end of the final breakage event. Additionally, Fig. 7b indicates that the last breakages event are spread over a wider set of regions, but still close to the first breakage sub-regions namely: B2, C2, A2, and A1.

Figure 7c presents the local values of breakage percentage in Region A for Re = 18,380. It can be seen that about 90% of first breakage occur at the blade's tip in sub-region A1a at the entry area of bubble to the impeller zone. In addition, the majority of last breakages occur close to the blade's tip at A1a and in between the blades at A2. Figure 7d, for Re = 40,830, shows that the majority of first breakages in sub-region A2 in between blades and in sub-region A1a. While, the majority of last breakages occur away from the blade's tip close to the bubble entry

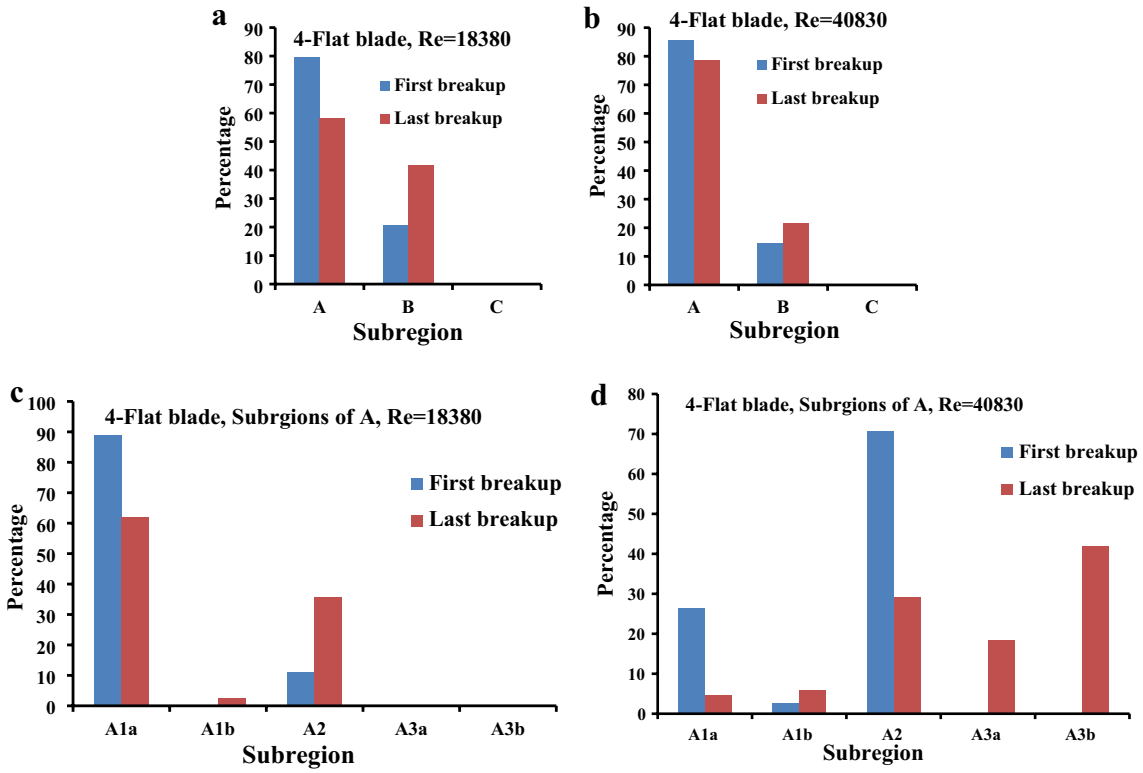

Fig. 7 Percentage of first and last breakage locations for the 4-flat blades impeller for **a** Re = 18,380 and **b** Re = 40,830. **c** Percentages of first and last breakages in sub-regions of A for 4-flat blades impeller at Re = 18,380. **d** Percentages of first and last breakages in sub-regions of A for 4-flat blades impeller at Re = 18,380

area in the sub-region A1b. Considerable percentages of last breakage occur at sub-region A2.

Comparing Figs. 7d and 5d indicates that the presence of four blades drive the mother bubble into region A2 which causes an increased number of first breakages at this region reaching 70%.

3.4 Twisted Blades Impeller

Figure 8a and b presents a series of images showing typical examples for breakages at different locations around the 4-twisted blades impeller.

The local breakage behavior of this twisted blades impeller is noticeably different from the flat bladed geometries. Figure 9a presents the breakage percent for the first and last breakage at the lower Re of 18,380. It can be seen that

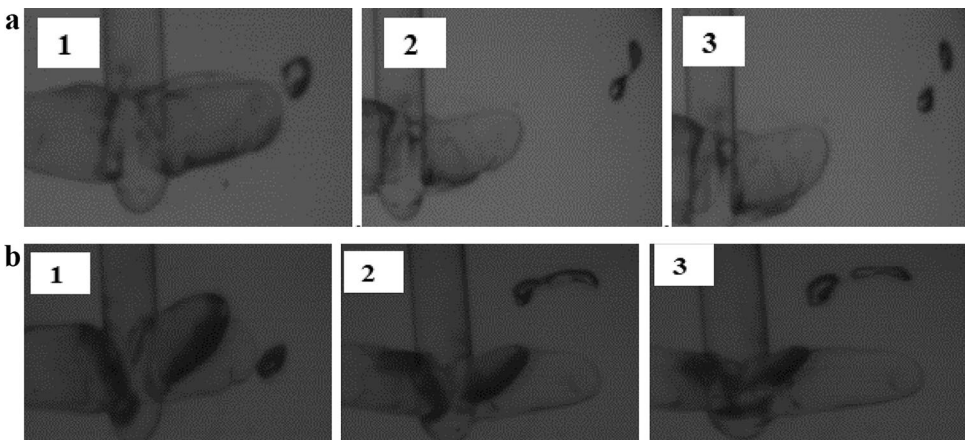

Fig. 8 **a** First breakage at sub-region A1, 4-twisted blades impeller, Re = 29,600. **b** First breakage at sub-region B1, 4-twisted blades impeller, Re = 29,600

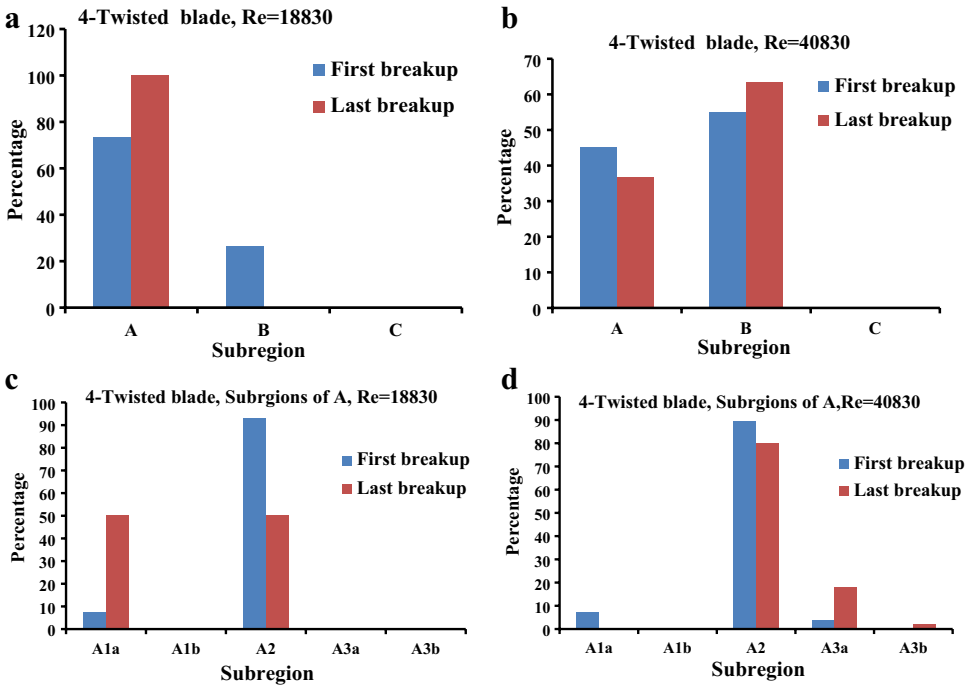

Fig. 9 **a** First and last breakage locations for the 4-twisted blades impeller for Re = 18,380. **b** First and last breakage locations for the 4-twisted blades impeller for Re = 40,830. **c** Percentages of first and last breakages in sub-regions of A for 4-twisted blades impeller at Re = 18,380. **d** Percentages of first and last breakages in sub-regions of A for 4-twisted blades impeller at Re = 18,380

68% of first breakages occur at B2 (often by collision with blades), 16% occur at B1, and 15% at A1 and A2. These higher breakage percentage sub-regions are different from that of the 2-flat and 4-flat bladed geometries. This is ascribed to the difference in the flow field around the impeller and that the inclined blade does not cause high shearing effects. The only two sub-regions of last breakage are B2 and A2 which are close to the main region of first breakages.

The two most active first breakage sub-regions for the higher Re are B1 and B2 each with 26%, followed by A1 with 19% as displayed in Fig. 9b. This is followed by 14% occurring in C2, then 11% in C1, then less than 5% for sub-regions A2, D1, and D2. The presence of the first breakage in sub-region D1 for this impeller is unique among the impellers that were tested. The first breakups in sub-regions B1, A1, D1 for other impeller geometries are few because most of the daughter bubble arrive to these areas are small in size.

Figure 9b shows that the last breakages for this twisted blades impeller are mainly occurring in B1, C2, and D1.

In general, most breakages occurring in Region 2 (refer to Fig. 2c) are by bubble–blade collisions, while that occurring in Regions 1 and 3 are by turbulent fluctuations and bubble–eddy collisions.

The occurrence of high first breakage percentage in these sub-regions away from the impeller (in B1, A1, D1) is attributed to the fact that the breakage probability for this impeller is relatively low and thus most mother bubbles pass the impeller region in its original released size which then results in breakage away from the impeller. It was reported by Hasan (2017b) that the energy required to break the larger bubbles is lower than that required for smaller bubbles because the cohesive forces of smaller bubble are higher.

3.5 Number of Daughter Bubbles

Figure 10 presents the average number of daughter bubbles (fragments) for the different impeller geometries for the three different Re investigated in this research. It shows that the number of fragments increases with increasing Re for all impeller geometries. In addition, the 4-flat blades impeller

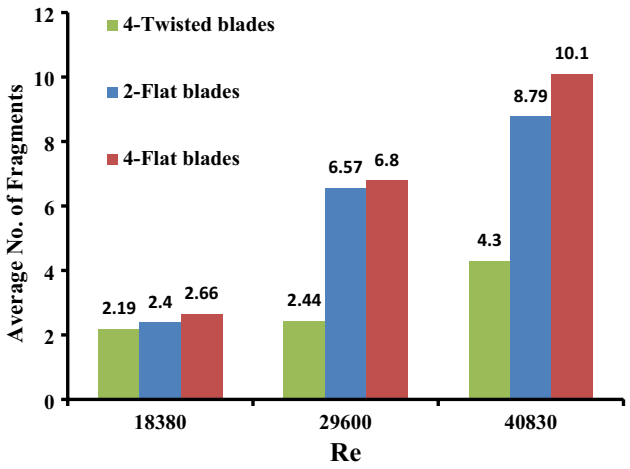

Fig. 10 Average number of fragments vs. Re for different impeller geometries

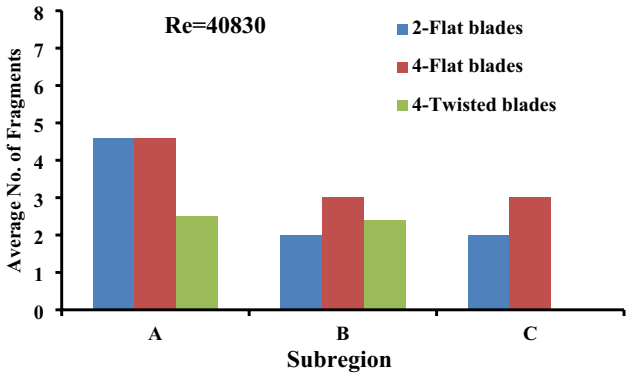

Fig. 11 Number of fragments for each main region around the impeller for Re = 40,830

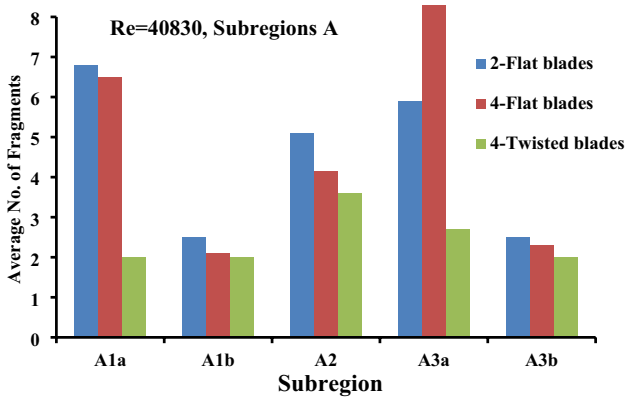

Fig. 12 Number of fragments for each sub-region for Re = 40,830

produces the highest number of fragments, followed the 2-flat blades impeller, and then the 4-twisted blades.

The local distribution of number of fragments for the 4 different impellers at highest Re is presented in Fig. 11. It is evident that the local number of fragments varies with impeller geometry. For all geometries, the highest number of fragments is produced at locations A close to the blades tips. The minimum number of fragments is produced at region C below the blades. These locations in front of the blades are characterized by high turbulence and energy level.

Figure 12 shows the local number of fragments in different sub-regions around the impeller. For 2-flat blades and 4-flat blades impellers geometries, Region A1a is characterized by high number of fragments while for 4-twisted blades, the highest number of fragments is produced at sub-region A3a. This considerable difference in the behavior of number of fragments of 4-twisted blades is ascribed the different hydrodynamics around the impeller. The flow patterns around the 4-twisted blades, drive the bubbles into sub-region A3a to break up producing higher number of fragments there.

For all of the impellers geometries investigated, observing Figs. 5, 6, 7, 8, 9. 10, 11, 12 indicates that the sub-regions with high breakage percentages (or number of breakages) do not necessarily produce the highest number of fragments. This can be explained as follows: the breakages occurring close to the blade are due to the effect of two mechanisms (Kumar et al. 1998; Liao and Lucas 2009; Zhang et al. 2020) namely; breakage by blade shearing effect and breakage by collision with the blades. However, the breakages occurring away from the blade are often caused by the effect of turbulent fluctuation (Andersson and Andersson 2006; Lalanne et al. 2019; Herø et al. 2020). The breakages caused by shear effect and by collision with the blade, produce a higher number of fragments than that by turbulent fluctuation, as has been observed by Alabdly et al. (2020). Therefore, the number of fragments in Region 2 is always higher than other regions because most breakages in this region occur by collisions with blades or by blade high shear effect.

The low number of fragments provided by the 4-twisted blades is ascribed to the low turbulence level (Alabdly et al. 2020). In addition, the inclined blades do not provide high enough shearing effect. The developed flow patterns caused by this geometry, push the bubble away from the blade which results in a low number of breakages.

Overall, for all impeller geometries investigated in this work, at low Re, the largest number of daughter bubbles are produced in Region 2, close to the blade's tip. This is considered to be because of the high shear effect within the continuous phase and the high probability of bubble collision with the blade.

A lower percentage of breakages occur in Region 1, above the impeller, because the bubble has already passed through Region 2 of high shearing effect and high turbulence level. It is subjected to the disruptive force during the passage through Region 2 which leads to a breakage in Region 1.

4 Conclusions

The impeller geometry affects the local behavior of bubble breakage in the stirred tank. The difference in breakage rate and number of fragments provided by different geometries is ascribed to the difference in the flow hydrodynamics around each geometry. At low Re, up to 90% of breakages occur at the blades tip, while at higher Re the breakage locations are varied around the impeller due to the effect rotational flow currents which translate the bubbles into different zones. For higher Re, the percentages of last breakages occurring above the blades increase due to the increased daughter bubbles dispersion. Low breakage percentages occur below the blades even at higher Re. The 4-flat blades impeller gives the largest number of daughter bubbles which are more uniformly distributed around the impeller than other

geometries. In general, for flat bladed impellers, the highest number of daughter bubbles is produced in front of blade tip. For 4-twisted bladed impellers, a considerable percentage of breakages (about 30%) occur in region above the blades. The number of breakages occurring and number of daughter bubbles produced below the blades are generally low.

Acknowledgements The authors acknowledge the contribution of alexander von Humboldt Foundation/Germany for providing experimental devices for performing this work.

References

Abbaszadeh M, Alishahi MM, Emdad H (2021) A new bubbly flow detection and quantification procedure based on optical laser-beam scattering behavior. Meas Sci Technol 32:025202

Alabdly H, Majdi H, Hamad M, Hathal M, Hasan BO (2020) Effect of impeller geometry on bubble breakage and the contributions of different breakage mechanisms in a stirred tank. J. fluid dynamic research 52:065504

Alves SS, Maia CI, Vasconcelos JMT, Serralheiro AJ (2020) Bubble size in aerated stirred tanks. Chem Eng J 3990:1–9

Ameur H (2020) Newly modified curved-bladed impellers for process intensification: energy saving in the agitation of Hershel-Bulkley fluids. Chem Eng Process Process Intensif 154:108009

Ameur H (2020b) Christophe Vialb, Modified scaba 6SRGT impellers for process intensification: Cavern size and energy saving when stirring viscoplastic fluids. Chem Eng Process 148:107795

Ameur H (2019) Some modifications in the Scaba 6SRGT impeller to enhance the mixing characteristics of Hershel-Bulkley fluids. Food Bioprod Process 117:302–309

Andersson R, Andersson B (2006) On the breakup of fluid particles in turbulent flows. AIChE J 52(6):2020–2030

Azizi HZ, Naghashzadegan M, Shorkri V (2019) Comparison of numerical methods for two-fluid model for gas-liquid transient flow regime and its application in slug modeling initiation. Iran J Sci Technol Trans Mech Eng 3:663–673

Buss A, Suleik A, Rugele K, Vanags J. CFD analysis of a stirred vessel bioreactor with double pitch blade and rushton type impellers. In: Proceedings of the 2017 COMSOL Conference in Rotterdam

Feng J, Cao J, Jiang J, Sun B, Cai Z, Gao Z (2019) Single bubble breakup in the flow field induced by a horizontal jet. Exp Res 17:1–10

Forgia N, Hero EH, Jakobsen HA (2021) High-speed image processing of fluid particle breakage in turbulent flow. Chem Eng Sci X12:100117

Hallaile M, Merchuk JC (2007) operation policies for a gas-liquid stirred tank reactor. Chem Eng Commun 46:179–196

Harriott SM (2001) Unit operations of chemical engineering, 6th edn. McGraw-Hill International, New York

Hartmann H, Derksen JJ, Montavon C, Pearson J, Hamill IS, van den Akker HEA (2004) Assessment of large eddy and RANS stirred tank simulations by means of LDA. Chem Eng Sci 59:2419–2432

Hasan BO, Krakau F (2017) Experimental study on the bubble breakage in a stirred tank. Part 1. Mechanism and effect of operating parameters. Int J Multiph Flow 97:94–108

Hasan BO (2018) Experimental study on the bubble breakage in a stirred tank, Part 2: Local dependence of breakage events. Exp Thermal Fluid Sci 96:48–62

Hasan BO, Hamad MF, Majdi HS, Hathal MM (2021) Experimental characterization of dynamic behavior of single bubble breakage in an agitated tank. Eur J Mech B/Fluid 85:430–443

Hasan BO (2017) Breakage of drops and bubbles in a stirred tank: a review of experimental studies. Chin J Chem Eng 25:698–711

Hero EH, Lorgia N, Solsvik J, Jakobsen HA (2020) Single drop breakage in turbulent flow: statistical data analysis. Chem Eng Sci 8:100082

Hinze JO (1955) Fundamentals of the hydrodynamic mechanism of splitting in dispersion processes. AIChE 1:289–295

Huchet F, Linea A, Morchaina J (2009) Evaluation of local kinetic energy dissipation rate in the impeller stream of a Rushton turbine by time-resolved PIV. Chem Eng Res Design 87:369–376

Kausley SB, Yadav MD, Dastane GG, Holkar CR, Pandit AB (2018) Process intensification opportunities in multiphase stirred tank reactors. Chem Ind Digest

Kumar S, Ganvir V, Satyanand C, Kumars R, Gandhi KS (1998) Alternative mechanisms of drop breakup in stirred vessels. Chem Eng Sci 53(18):3269–3280

Lalanne BO, Masbernat F (2019) Risso, A model for drop and bubble breakup frequency based on turbulence spectra. AIChE J 65:347–359

Liao Y, Lucas D (2009) A literature review of theoretical models for drop and bubble breakup in turbulent dispersions. Chem Eng Sci 65(10):2851–2864

Maass S, Kraume M (2012) Determination of breakage rates using single drop experiments. Chem Eng Sci 70:146–164

Maass S, Eppinger T, Altwasser S, Rehm T, Kraume M (2011) Flow field analysis of stirred liquid-liquid systems in slim reactors. Chem Eng Technol 34(8):1215–1227

Martin M, Montes F, Galan M (2008) Influence of impeller type on the bubble breakup process in stirred tanks. Ind Eng Chem Res 47:6251–6263

Mesa D, Brito-Parada PR (2020) Bubble size distribution in aerated stirred tanks: quantifying the effect of impeller-stator design. Chem Eng Res Design 160:356–369

Moffat RJ (1988) Describing the uncertainties in experimental results. Exp Therm Fluid Sci 1:3–17

Oliveira M, Fitch AW, Ni X (2003) A study of bubble velocity and bubble residence time in a gassed oscillatory baffled column effect of oscillation frequency. Trans IChemE 81:233–242

Shi X, Tan Chao, Feng Dong MJD, Silva, (2020) Conductance sensors for multiphase flow measurement: a review. IEEE Sens J 21:11

Slaiman QJM, Hasan BO, Mahmood H A (2008) Corrosion inhibition of carbon steel under two-phase flow (water-petroleum) simulated by turbulently agitated system. Can J Chem Eng 86(2):240–248

Solsvik J, Jakobsen HA (2015) Single air bubble breakup experiments in stirred water tank. Int J Chem React Eng 13:477–491

Solsvik J, Maass S, Jakobsen H (2016) Definition of the single drop breakup event. Ind Eng Chem Res 55:2872–2882

Zamiri A, Chung JT (2018) Numerical evaluation of turbulent flow structures in a stirred tank with a Rushton turbine based on scale-adaptive simulation. Comput Fluids 170:236–248

Zhang H, Yang G, Sayyar A, Wang T (2020) An improved bubble breakup model in turbulent flow. Chem Eng J 386:121484